Cation Exchange in Dynamic 3D Porous Magnets: Improvement of the Physical Properties

ARTICLE *in* INORGANIC CHEMISTRY · OCTOBER 2015

Impact Factor: 4.76 · DOI: 10.1021/acs.inorgchem.5b01854

Inorganic Chemistry

Article

pubs.acs.org/IC

Cation Exchange in Dynamic 3D Porous Magnets: Improvement of the Physical Properties

Thais Grancha,[†] Alvaro Acosta,[†] Joan Cano,[†,‡] Jesús Ferrando-Soria,*[,†] Beatriz Seoane,[§] Jorge Gascon,[§] Jorge Pasán,[⊥] Donatella Armentano,*[,∥] and Emilio Pardo*[,†]

[†]Departament de Química Inorgànica, Instituto de Ciencia Molecular (ICMOL), and [‡]Fundació General de la Universitat de València (FGUV), Universitat de València, 46980 Paterna, València, Spain

[§]Catalysis Engineering-Chemical Engineering Department, Delft University of Technology, Julianalaan 136, 2628 BL Delft, The Netherlands

[⊥]Laboratorio de Rayos X y Materiales Moleculares, Departamento de Física Fundamental II, Universidad de La Laguna, E−38201 Tenerife, Spain

[∥]Dipartimento di Chimica e Tecnologie Chimiche, Università della Calabria, Rende 87036, Cosenza, Italy

Supporting Information

ABSTRACT: We report two novel three-dimensional porous coordination polymers (PCPs) of formulas $Li_4\{Mn_4[Cu_2(Me_3mpba)_2]_3\}\cdot 68H_2O$ (**2**) and $K_4\{Mn_4[Cu_2(Me_3mpba)_2]_3\}\cdot 69H_2O$ (**3**) obtained—via alkali cation exchange in a single-crystal to single-crystal process—from the earlier reported anionic manganese(II)−copper(II) PCP of formula $Na_4\{Mn_4[Cu_2(Me_3mpba)_2]_3\}\cdot 60H_2O$ (**1**) [Me_3mpba^{4-} = *N*,*N*′-2,4,6-trimethyl-1,3-phenylenebis(oxamate)]. This postsynthetic process succeeds where the direct synthesis in solution from the corresponding building blocks fails and affords significantly more robust PCPs with enhanced magnetic properties [long-range 3D magnetic ordering temperatures for the dehydrated phases (**1**′−**3**′) of 2.0 (**1**′), 12.0 (**2**′), and 20.0 K (**3**′)]. Changes in the adsorptive properties upon postsynthetic exchange suggest that the nature, electrostatic properties, mobility, and location of the cations within the framework are crucial for the enhanced structural stability. Overall, these results further confirm the potential of postsynthetic methods (including cation exchange) to obtain PCPs with novel or enhanced physical properties while maintaining unaltered their open-framework structures.

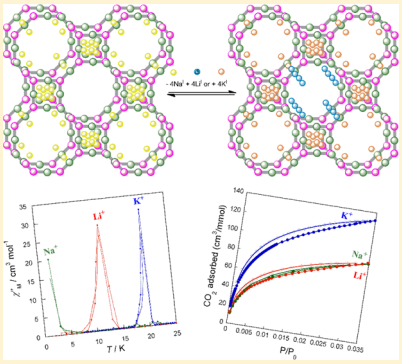

INTRODUCTION

The preparation of new examples of high-dimensional porous coordination polymers (PCPs), which are often called metal−organic frameworks (MOFs),[1−6] attracts the interest of many groups because of the great diversity of properties they can present.[7−12] PCPs are especially appealing for the design of the so-called multifunctional magnetic materials (MMMs),[13−15] where they combine magnetic properties with other essential properties in the field of nanotechnology.[16] For example, in the intercrossing area of MOF chemistry and molecular magnetism, the modulation of the magnetic properties of the host coordination framework is a hot topic. A rational route is the inclusion of particular guests such as neutral solvent molecules or gases and charged anions or cations through physi- or chemisorption processes, opening vast perspectives for this class of PCP-based porous magnets as magnetic sensors.

These rationally designed hybrid materials—consisting of metal ions or small coordination complexes linked by diverse organic or metallo-organic bridging ligands yielding two- (2D) or three-dimensional (3D) networks of varying topologies—show void channels as a remarkable common structural characteristic. In fact, the presence of these variable-size channels in their open-framework structure, which can be occupied by guest cations and anions or neutral solvent molecules, is ultimately responsible for their intriguing physical properties as well as for a fascinating host−guest chemistry.[17]

Total control of the PCP structure by using either hydro(solvo)thermal or rationally programmed soft-chemical methods is not always feasible, as many factors can interfere in the assembly process.[18] Alternatively, postsynthetic (PS) methods[19,20] can be helpful to gain control from a structural point of view and, thus, pave the way to the functionalization of a given PCP with the desired architecture, either to improve its properties or to incorporate new functionalities without altering its structure. Among the different possibilities that PS methods can offer (including transmetalation processes,[21,22] ligand exchange,[23] etc.), the exchange of guest molecules hosted in the pores of the PCPs[24,25] has emerged as the most straightforward way to improve properties such as magnetism,[26,27] gas adsorption,[28−37] catalysis,[38,39] drug delivery,[40] or luminescence.[41,42] Anionic oxamato-based coordination poly-

Received: August 18, 2015

DOI: 10.1021/acs.inorgchem.5b01854
Inorg. Chem. XXXX, XXX, XXX−XXX

mers[43−47] can be of potential interest in some or all of the aforementioned points.

RESULTS AND DISCUSSION

In an earlier communication, we reported the first porous magnet of the bimetallic oxamate family of formula $Na_4\{Mn_4[Cu_2(Me_3mpba)_2]_3\}\cdot 60H_2O$[45] (**1**) [$Me_3mpba^{4-}$ = *N*,*N*′-2,4,6-trimethyl-1,3-phenylenebis(oxamate)]. In this work, we report the crystal structures and magnetic and gas sorption properties of two novel porous magnets of formulas $Li_4\{Mn_4[Cu_2(Me_3mpba)_2]_3\}\cdot 68H_2O$ (**2**) and $K_4\{Mn_4[Cu_2(Me_3mpba)_2]_3\}\cdot 69H_2O$ (**3**). **2** and **3** are obtained via alkali cation exchange[28−42] from the previously reported ancestor **1** in a single-crystal to single-crystal (SC−SC) process (Scheme 1). Interestingly, this straightforward postsynthetic replacement of the Na^+ cations in **1** by Li^+ (**2**) or K^+ (**3**) cations enhances the robustness of the novel MOFs, and an overall improvement in both the gas sorption and the magnetic properties is observed.

Scheme 1. Cation Exchange Process for the Replacement of the Sodium(I) Ions (Yellow Spheres) in the Anionic Square/Octagonal Pillared Network of 1 with Lithium(I) (2) or Potassium(I) (3) Ions (Blue and Orange Spheres)

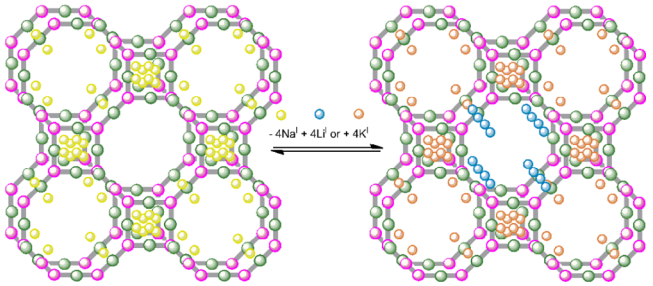

Synthesis and X-ray Crystal Structure. **1** was prepared as reported earlier[45] by slow diffusion in water of the preformed dicopper(II) complex $Na_4[Cu_2(Me_3mpba)_2]\cdot 4H_2O$ and $Mn(NO_3)_2\cdot 4H_2O$ (3:4 molar ratio) in an H-shaped tube at room temperature. **2** and **3** were obtained by immersing crystals of **1** in saturated aqueous solutions of $LiCl\cdot 6H_2O$ and $KCl\cdot 6H_2O$, respectively. Although ICP-AES measurements and SEM microscopy indicate that the majority of the cations are exchanged in a few minutes, preventing any possible kinetic analysis, the crystals were left in the saturated solutions for 24 h to ensure the complete replacement (see Experimental Section). Preliminary experiments point toward the reversibility of the process. The structures of **2** and **3** could be determined by X-ray diffraction on single crystals, revealing thus the occurrence of a unique SC−SC transformation upon alkali metal substitution in the solid state (see Experimental Section).

1−**3** are isostructural (Table S1, Supporting Information), and they consist of an anionic 3D $Mn^{II}_4Cu^{II}_6$ open-framework structure exhibiting a pillared square/octagonal layer structural architecture containing either small square channels or large octagonal pores along the *c* axis (Figure 1). The presence of two different types of narrow and wide octagonal pores (relative diameters of ca. 1.5 and 2.0 nm) arises from the different disposition of the trimethyl-substituted phenylene spacers directing inward or outward of the voids, respectively.

The hydrated charge-counterbalancing alkali M^I cations [M = Na (**1**), Li (**2**), and K (**3**)] exhibit a different distribution within the channels, along both the parallel and perpendicular

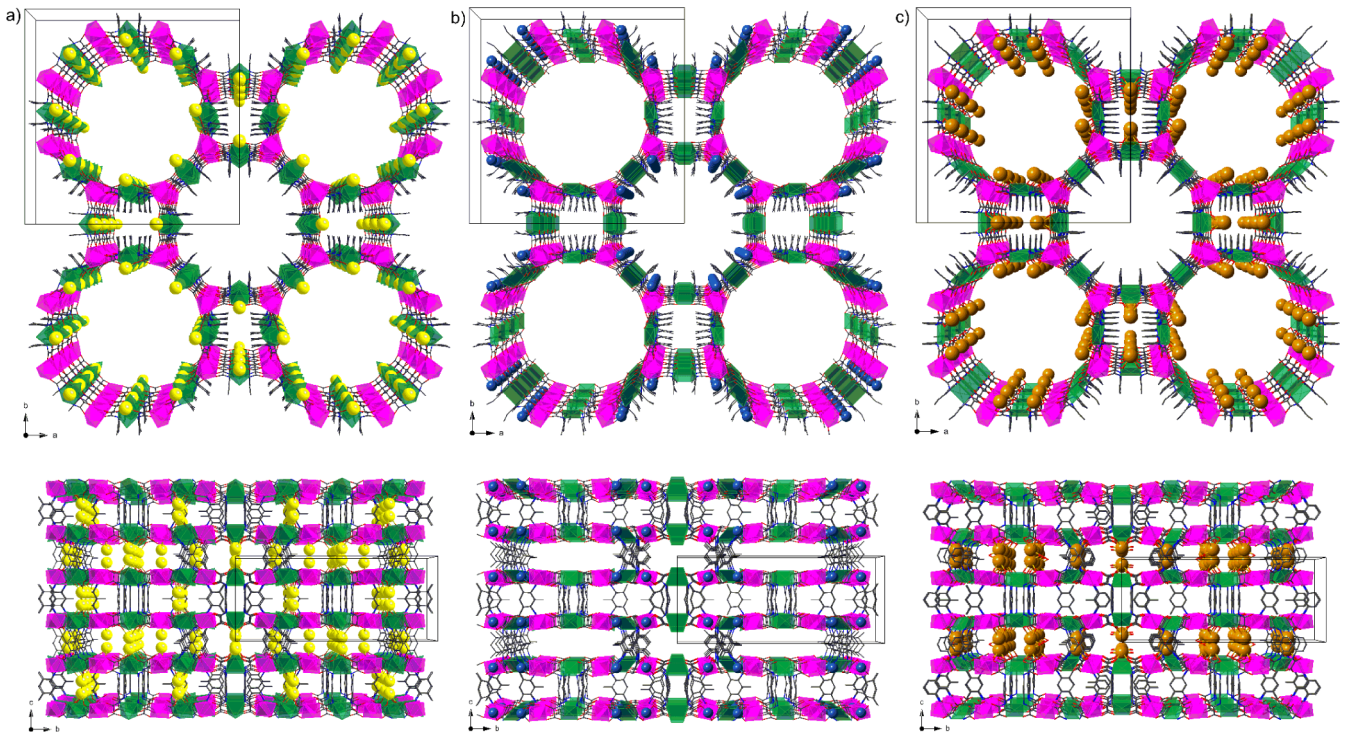

Figure 1. Perspective view of the 3D anionic network of **1** (a), **2** (b), and **3** (c) along the crystallographic *c* (top) and *a* (bottom) axes. Copper and manganese atoms from the covalent network are represented by green and purple polyhedra, respectively, whereas the sodium (**1**), lithium (**2**), and potassium (**3**) atoms occupying the channels are depicted as yellow, blue, and orange spheres, respectively (free and coordinated water molecules are omitted for clarity).

DOI: 10.1021/acs.inorgchem.5b01854
Inorg. Chem. XXXX, XXX, XXX−XXX

directions most likely as a consequence of the variation in the ionic radii of these cations [0.68 (Li^+), 0.95 (Na^+), and 1.33 Å (K^+)]. While the small-sized Li^+ ions occupy only the narrow octagonal channels in **2**, the bigger Na^+ and K^+ occupy the square and wide octagonal channels in **1** and **3**, respectively (Figure 1a–c, top). Moreover, Li^+ ions are located in the intralayer space in **2**, whereas Na^+ and K^+ occupy the interlayer space in **1** and **3**, respectively (Figure 1a–c, bottom). This different location of the alkali metal ions must lie at the origin of the enhanced structural stability in **2** and **3** compared to **1**. Thus, although all M^I ions are weakly coordinated to the carboxylate- and/or carbonyl-oxygen atoms from the coordination network [M–O = 2.410(10)–2.883(12) (**1**), 1.925(14)–2.186(16) (**2**), and 2.683(11)–2.844(9) Å (**3**)], they coordinate in different positions. This fact, together with the different nature of the cations, plays a key role in the structural integrity or collapse upon solvent loss (Figures S1 and S2, Supporting Information).

Figures S1a and S2a show that Na1 and Na2 atoms, which are located in the larger octagonal pores, also full of water molecules, are simultaneously coordinated to the carboxylate-oxygen atoms from the two Me_3mpba ligands, forming the copper(II) basal plane. Upon water removal, this feature can originate a significant tetrahedral distortion of the square planar Cu^{II} ions, which would originate a reorientation of the organic linkers, ultimately leading to the structural collapse. This tetrahedral distortion of the copper(II) ions has already been reported for other oxamato-based PCPs.[44] In contrast, Li and K atoms in **2** and **3**, respectively, are coordinated to the carbonyl-oxygen atoms that form the coordination environment of the octahedral manganese(II) ions (Figures S1b,c and S2b,c). The possible distortions in the Mn^{II} octahedral geometry originated by displacements of the coordinated Li or K atoms when losing the water molecules would be much softer than those predicted for a square-planar to tetrahedral distortion and would not lead to a final structural collapse.

The estimated empty volumes without the highly disordered crystallization water molecules are slightly different for all three compounds [11997 (**1**), 13109 (**2**), and 12204 $Å^3$ (**3**)], and they represent up to 60%, 63.1%, and 55.8% for **1**, **2**, and **3**, respectively, of potential void per unit cell volume [V = 20075 (**1**), 20770 (**2**), and 21868 $Å^3$ (**3**)].

Thermogravimetric Analysis. The water contents of **1**–**3** are established by thermogravimetric analysis (TGA) under a dry N_2 atmosphere. A fast mass loss from room temperature to around 150 °C can be observed for all three compounds, followed by a *plateau* in the range ca. 150–300 °C, and then decomposition starts (Figure S3). The mass loss values of ca. 31% (**1**), 34% (**2**), and 35% (**3**) at 125 °C correspond to 60, 68, and 69 H_2O molecules per formula unit, respectively.

X-ray Powder Diffraction. The powder X-ray diffraction (PXRD) patterns of polycrystalline samples of the hydrated phases of **1**–**3** were measured in water suspensions to prevent the partial loss of water at room temperature (Figures 2 and S4–S6). Within each sample, the experimental PXRD pattern profiles are well consistent with the calculated ones (Figure 2), confirming the pureness of the bulk samples. Moreover, the comparison of the PXRD patterns of **1**–**3** further confirms that all three compounds are isostructural (Figure 2) and, thus, that the exchange process of the alkali metal does not modify the open-framework structures, as revealed by the single-crystal X-ray structures.

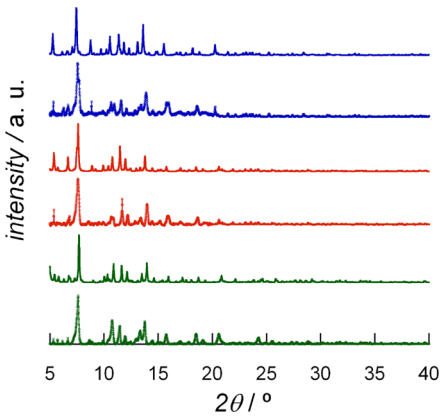

Figure 2. Experimental (—) and calculated (-O-) XRPD pattern profiles of the hydrated phases of **1** (green), **2** (red), and **3** (blue) measured as water suspensions in the 2θ range 5.0–40.0° at rt.

PXRD studies were then carried out for **1**–**3** in the temperature range 298–370 K to analyze the relative structural stability of each compound upon water loss (Figures 3 and S7–S10). The observed behavior is consistent with that predicted from the analysis of the crystal structures. After dehydration, variable-temperature PXRD patterns show a total loss of crystallinity for **1**, even at room temperature (Figure 3a). In contrast, the PXRD patterns of the activated phases of **2** and **3** show retention of crystallinity over the whole range of temperatures studied. Indeed, while **1** seems to amorphize upon removal of water, covalent networks of **2** and **3** remain crystalline, suggesting a very important role of the weak coordinative interactions with the diverse alkali countercations.

Gas Sorption Behavior. All samples of **1**–**3** were activated (dehydrated) at 80 °C under reduced pressure for 16 h prior to the sorption measurements (Figure 4), to give the dehydrated phases **1′**–**3′**.

The low-pressure N_2 adsorption isotherms at 77 K for **1′**–**3′** show remarkable differences. While the original **1′** displays hardly any adsorption of N_2, its lithium(I) (**2′**) and potassium(I) (**3′**) derivatives exhibit a much higher uptake (Figure 4a). For compounds **2′** and **3′**, the calculated Brunauer–Emmett–Teller (BET) surface areas [270 (**2**) and 200 m^2/g (**3**)] follow the trend expected according to the estimated volumes (see structural discussion above).

A similar trend to that of N_2 adsorption is observed for high-pressure H_2 isotherms measured at 77 K. In contrast, adsorption isotherms of CO_2 and CH_4 (both at 273 K) indicate that **1′** and **2′** have comparable porosities (see the almost overlapping CO_2 isotherms). We attribute these results to the amorphization of **1′** upon dehydration, which obviously leads to a less ordered structure with slightly smaller and less homogeneous pores that cannot be probed by N_2 at 77 K but are still accessible to smaller molecules such as CO_2. When comparing the adsorptive behavior of **2′** and **3′**, it is striking to observe that while the Li^+-containing sample displays a larger BET area, the K^+ sample shows a much higher affinity for H_2, CO_2, and CH_4. These results demonstrate that both the nature and location of the cation within the framework are of fundamental importance in the adsorptive properties of the material, in clear analogy to zeolites.[48]

Interestingly, these different uptake results for different adsorbates evidence that we are capable of achieving an important increase in the sorption capacity in a given material

DOI: 10.1021/acs.inorgchem.5b01854
Inorg. Chem. XXXX, XXX, XXX–XXX

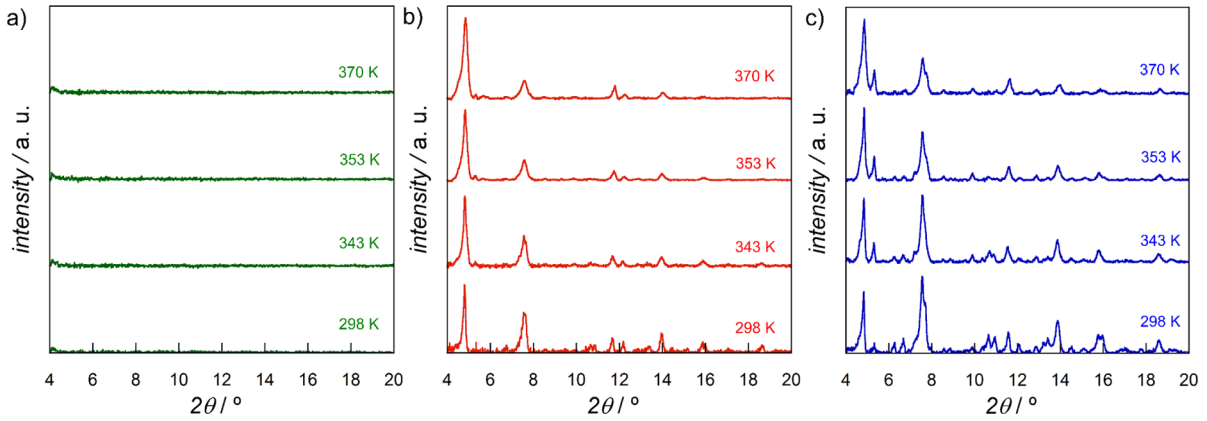

Figure 3. Variable-temperature XRD patterns of dehydrated **1** (a), **2** (b), and **3** (c) at 298, 343, 353, and 370 K.

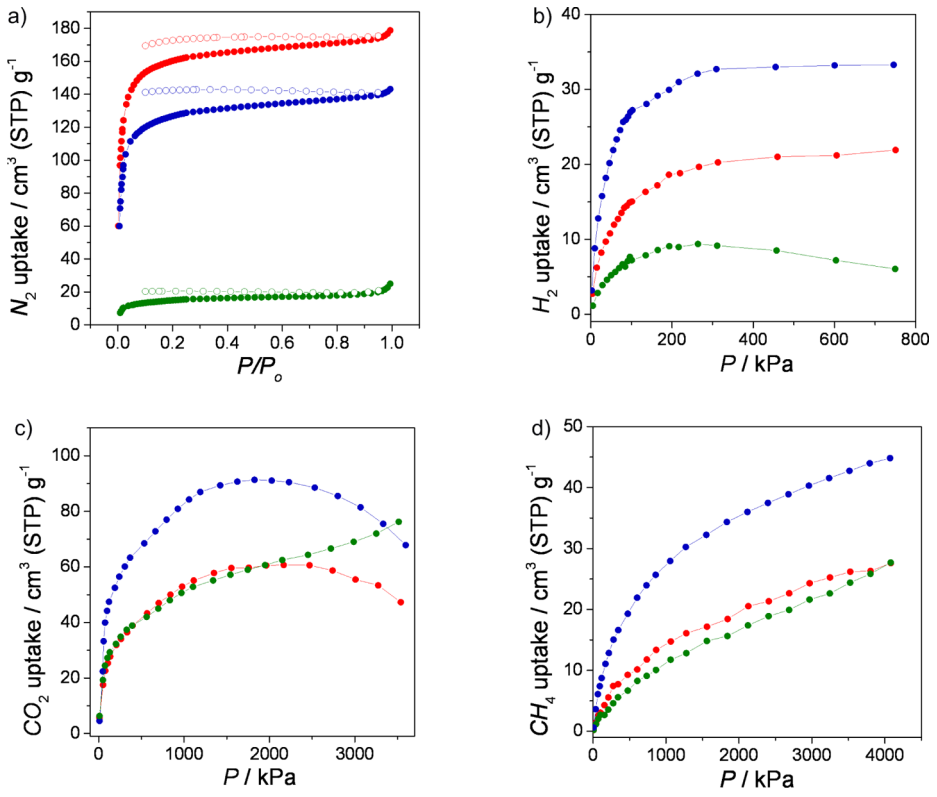

Figure 4. Low-pressure N_2 (a, 77 K) and high-pressure H_2 (b, 77 K), CO_2 (c, 273 K), and CH_4 (d, 273 K) sorption isotherms for **1′** (green), **2′** (red), and **3′** (blue). Filled and empty symbols indicate the adsorption and desorption isotherms, respectively. All samples were activated at 80 °C under reduced pressure for 16 h prior to carrying out the sorption measurements.

via cation exchange but, more importantly, and they reveal that we can also modify the gas selectivity.

Magnetic Properties. In order to analyze the effect of the alkali countercation replacement and the water loss along this series in the magnetic properties, we measured them in both the direct current (dc) and alternating current (ac) regimes (see Experimental Section), for both the hydrated samples **1**−**3** and their dehydrated phases **1′**−**3′**.

The $\chi_M T$ vs T plots (where χ_M is the dc molar magnetic susceptibility per $Cu^{II}_6Mn^{II}_4$ unit and T the temperature) for both **1**−**3** and **1′**−**3′** show the same qualitative general behavior (Figures S11 and S12). They exhibit a characteristic minimum indicative of a ferrimagnetic behavior as a consequence of the intralayer antiferromagnetic interactions between the Cu^{II} and high-spin Mn^{II} ions through the oxamato bridge, as previously found in other oxamato-based manganese(II)−copper(II)-layered compounds.

This common ferrimagnetic behavior of **1**−**3** was also suggested by the M vs H plots at 2.0 K (where M is the magnetization per $Cu^{II}_6Mn^{II}_4$ unit and H the applied dc magnetic field), which reveal, however, non-negligible differences between the hydrated and the dehydrated phases (Figure 5). The isothermal magnetization curves for **1**−**3** rapidly saturate at low field values, exhibiting maximum M values at 5 T, close to the calculated value of the saturation magnetization for the antiparallel spin alignment of the high-spin Mn^{II} (S_{Mn} = 5/2) and Cu^{II} (S_{Cu} = 1/2) ions [$M_s = (4g_{Mn}S_{Mn} - 6g_{Cu}S_{Cu})N\beta$ = 13.90 $N\beta$ with g_{Mn} = 2.0 and g_{Cu} = 2.1] (Figure 5a). In contrast, the isothermal magnetization curves for the dehydrated phases **1′**−**3′** do not saturate even at high fields,

DOI: 10.1021/acs.inorgchem.5b01854
Inorg. Chem. XXXX, XXX, XXX−XXX

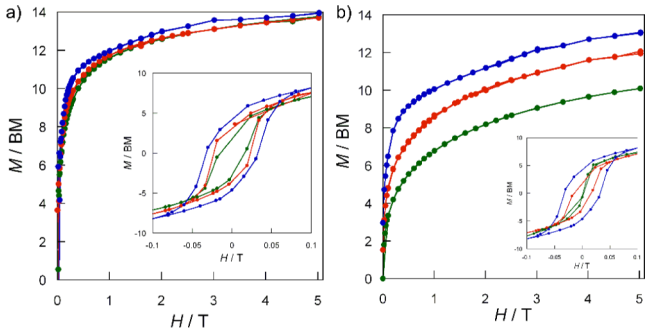

Figure 5. Field dependence of the magnetization (M) of **1**−**3** (a) and **1′**−**3′** (b). **1**, **1′** (green), **2**, **2′** (red), and **3**, **3′** (blue) at T = 2.0 K. The insets show in detail the hysteresis loops. The solid lines are only guides to the eye.

the maximum M values at 5 T being lower than the calculated saturation magnetization and dependent on the nature of the alkali countercation (Figure 5b). In addition, **1**−**3** show magnetic hysteresis loops with rather similar but low values of the coercive magnetic field around 400 G (inset of Figure 5a), whereas those of the dehydrated phases decrease from **3′** to **2′** and almost vanish for **1′** (inset of Figure 5b).

These differences in the magnetic behavior between **1**−**3** and **1′**−**3′** can be observed in the field-cooled magnetization (FCM) vs T plots (Figure S13). While the FCM curves of the hydrated phases show abrupt increases indicative of a long-range magnetic ordering at around 20.0 K for all three compounds (Figure S13a), those of the dehydrated phases shift continuously to lower temperatures following the trend **3′** > **2′** > **1′** (Figure S13b). This is further confirmed by the χ_M'' vs T plots (where χ_M'' is the out-of-phase ac molar magnetic susceptibility per formula unit) of **1**−**3** (Figure 6). Hence, a

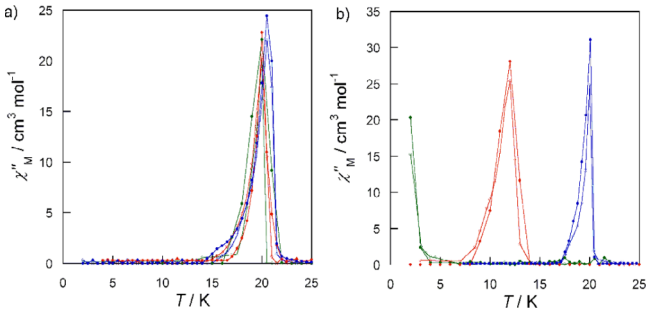

Figure 6. Temperature dependence of the ac out-of-phase molar magnetic susceptibility (χ_M'') of **1**−**3** (a) and **1′**−**3′** (b). **1**, **1′** (green), **2**, **2′** (red), and **3**, **3′** (blue) with a ±4.0 G field oscillating at 1000 (-●-) and 100 (-○-) Hz, respectively.

sharp frequency-independent peak occurs for **1**−**3** at a common critical temperature (T_C) value of 20.0 K (Figure 6a). Instead, the T_C values for the dehydrated phases decrease from 20.0 (**3′**) to 12.0 (**2′**) and then to below 2.0 K (**1′**) (Figure 6b).

Interestingly, the variation found in the long-range 3D magnetic ordering between **1**−**3** and **1′**−**3′** reflects the observed differences in the robustness of each compound upon water loss, as revealed by the PXRD studies. So, the T_C value shifts from 20.0 K to below 2.0 K for the sodium(I) derivative (**1′**), which is probably related to the aforementioned partial collapse of the network structure upon water removal. In contrast, the lithium(I) derivative (**2′**) exhibits a much softer decrease of the T_C value from 20.0 to 12.0 K, while the T_C value for the potassium(I) derivative (**3′**) remains unaltered, confirming thus the robustness of the network structure upon water removal.

CONCLUSIONS

In summary, we report a unique family of PCPs obtained in an SC to SC process via cation exchange. This process induces enhanced structural stability in the final materials, which is ultimately responsible for the severe improvement of both the magnetic and gas sorption properties upon solvent removal. In addition, the whole process has been followed by single-crystal X-ray diffraction, allowing comprehensive evidence, through structural insights, about the putative role of alkali metal ions on the structural stability of the materials and situating this work as one of the very first deep studies of cation-exchanged MOFs, reached with the help of single-crystal X-ray crystallography methods. Overall, the exchange of the sodium(I) countercations hosted in the channels by lithium(I) or potassium(I) results in more robust materials and affects dramatically their physical properties. On one hand, an important enhancement of the long-range 3D magnetic ordering temperatures for **2′** and **3′** has been observed. On the other hand, the nature and location of the cations within the framework determine the gas adsorption properties of the PCP. Our results give additional evidence that postsynthetic methods can be effectively used to modulate the physical properties of PCPs without altering their structures. Current efforts are dedicated to explore the ion exchange ability of these dynamic porous magnets toward toxic cations (radioactive and heavy metals) for future use of oxamato-based coordination polymers as detoxification agents.

EXPERIMENTAL SECTION

Materials. $Na_4[Cu_2(Me_3mpba)_2]\cdot 4H_2O$ was synthesized according to literature methods.[45] All chemicals were of reagent grade quality, and they were purchased from commercial sources and used as received.

Preparation of $M_4\{Mn_4[Cu_2(Me_3mpba)_2]_3\}\cdot nH_2O$ [1: M = Na^+ (*n* = 60); 2: M = Li^+ (*n* = 68); 3: M = K^+ (*n* = 69)]. X-ray quality bright green prisms of **1** were grown by slow diffusion of aqueous solutions prepared with stoichiometric amounts of $Na_4[Cu_2(Me_3mpba)_2]\cdot 4H_2O$ (0.011 g, 0.015 mmol) and $Mn(NO_3)_2\cdot 4H_2O$ (0.005 g, 0.020 mmol) in an H-shaped tube on standing at room temperature after 4 weeks. Well-formed pale green prisms of **2** and **3**, which were suitable for X-ray diffraction, were then obtained by immersing crystals of **1** for 24 h in saturated aqueous solutions of $LiCl\cdot 6H_2O$ and $KCl\cdot 6H_2O$, respectively. Yield: 0.010 g, 58%. Anal. Calcd (%) for $C_{78}H_{180}N_{12}O_{96}Na_4Cu_6Mn_4$ (3515.3): C 26.65, H 5.16, N 4.78. Found: C 26.59, H 5.11, N 4.78. IR (KBr): 1602 cm^{-1} (CO). **2**: Yield: 97%. Anal. Calcd (%) for $C_{78}H_{196}N_{12}O_{104}Li_4Cu_6Mn_4$ (3595.2): C 26.06, H 5.49, N 4.67. Found: C 26.19, H 5.71, N 4.66. IR (KBr): 1599 cm^{-1} (CO). **3**: Yield: 98%. Anal. Calcd (%) for $C_{78}H_{198}N_{12}O_{105}K_4Cu_6Mn_4$ (3741.8): C 25.04, H 5.33, N 4.49. Found: C 25.01, H 5.42, N 4.47. IR (KBr): 1600 cm^{-1} (CO).

Single-Crystal X-ray Diffraction. Single crystals of **2** and **3** were mounted on glass fibers, in a grease drop, and very quickly placed on a liquid nitrogen stream cooled at 100 K to avoid the degradation upon dehydration. Diffraction data were collected on a Bruker-Nonius X8APEXII CCD area detector diffractometer using graphite-monochromated Mo K_α radiation (λ = 0.710 73 Å). The data were processed through the SAINT[49] reduction and SADABS[50] multiscan absorption software. As previously reported, crystals of **2** and **3**, suitable for X-ray diffraction, were obtained by immersing crystals of **1** for 24 h in saturated aqueous solutions of $LiCl\cdot 6H_2O$ and $KCl\cdot 6H_2O$,

DOI: 10.1021/acs.inorgchem.5b01854
Inorg. Chem. XXXX, XXX, XXX−XXX

respectively, after a crystal-to-crystal transformation accounting for a poor quality and a poor diffraction power of the samples with respect to **1** (Figure S14). In fact, a lower θ_{max} of diffraction was obtained (detected as Alerts A in the checkcifs of **2** and **3**), especially for **2**, even if many efforts were made to extract the best diffraction data from each sample. However, the solution and refinement parameters are suitable, compared with analogue MOF structures previously reported; thus we are convinced that the structures found are consistent.[51−54]

The structures were solved by the Patterson method and subsequently completed by Fourier recycling using the SHELXL-2013 software package.[55,56] In **2**, to increase the data/parameters ratio, only the metal atoms were refined anisotropically, while in **3** all non-hydrogen atoms were refined anisotropically except K^+ alkali metal, for which four positions have been refined, with 0.15 (K1a), 0.20 (K1b), 0.15 (K1c), and 0.5 (K2) occupancy factors, and disordered water molecules. The hydrogen atoms were set in calculated positions and refined as riding atoms. The high thermal vibration parameters (Alerts A and B in the checkcifs) displayed for atoms in the organic ligand are a consequence of contributions from different factors, including (a) the flexibility of the framework and consequential disorder, (b) the high residual electron density produced by the methyl groups that are dynamic components of the walls, (c) the use of some bond length and angle restraints during the refinements or fixed positions of some highly disordered atoms, and (d) above all the limitation in the data quality, coming from crystals obtained upon postsynthetic exchange. Furthermore, and as expected for such systems, the lattice water molecules were highly disordered and cannot be satisfactorily modeled (at the origin of the first-level Alerts A in **2** and **3**). The rare structures found from the ΔF map were refined with constraints, and their hydrogen atoms were generally neither found nor calculated. As a consequence, in both compounds **2** and **3** the contribution to the diffraction pattern from the highly disordered water molecules of crystallization (272 molecules of H_2O in **2** and 276 in **3** located in the voids of the lattice that amount to 60% percentage void volume of the unit cell) was subtracted from the observed data through the SQUEEZE method, implemented in PLATON.[57] The final formulation for each compound is consistent with the residual electron density and volume. The final full-matrix least-squares refinements on F^2, minimizing the function $\sum w(|F_o| - |F_c|)^2$, reached convergence with the values of the discrepancy indices given in Table S1. High R values (levels Alert A in checkcifs) are, most likely, mainly affected by the contribution of the highly disordered solvent to the intensities of the low-angle reflections. The final geometrical calculations and all the graphical aspects were carried out with CRYSTAL MAKER, WinGX, and POV-Ray programs.[58−60]

X-ray Powder Diffraction. Polycrystalline samples of **1**−**3** were prepared by introducing the corresponding sample into 0.5 mm borosilicate capillaries and then mounted and aligned on an Empyrean PANalytical powder diffractometer, equipped with a Cu Kα radiation (λ = 1.540 56 Å). For each sample, five measurements were collected at room temperature (2θ = 2−50°) and merged in a single diffractogram. The collected data were analyzed with the X'Pert HighScore Plus software.[61]

Variable-temperature PXRD studies were also carried out following the same procedure for solid polycrystalline samples of **1**−**3**. In this case, three repeated measurements were collected for each sample (2θ = 4−20°) at different temperatures (298, 343, 353, and 370 K) and merged in a single diffractogram. Each measurement was carried out after waiting 10 extra minutes once the corresponding temperature was stabilized. The chosen narrower angle interval (2θ = 4−20°) obeys equipment safety reasons when using the cryostat and given the lack of important peaks beyond that range.

Thermogravimetric Analysis. The TGA measurements were carried out on crystalline samples of **1**−**3** under a dry N_2 atmosphere with a Mettler Toledo TGA/STDA 851^e thermobalance operating at a heating rate of 10 °C min^{-1}.

Gas Sorption. Low-pressure N_2 adsorption isotherms at 77 K were measured on crystalline samples of **1**−**3** in a Tristar II 3020 Micrometrics equipment. Prior to the measurements, the adsorbent was outgassed at 80 °C under N_2 flow for 16 h. The BET model was used to estimate the surface areas.[62]

High-pressure adsorption isotherms of CO_2, CH_4, and H_2 (purity of 99.995%) were determined using the volumetric technique with an apparatus from BEL Japan (Belsorp HP). Samples of **1**−**3** (ca. 0.2 g) were placed in the sample container, and they were pretreated by increasing the temperature to 363 K at a rate of 10 K/min under vacuum and maintaining the temperature for 2 h prior to their analysis.

Magnetic Measurements. Variable-temperature direct current and alternating current magnetic susceptibility measurements were carried out with a Quantum Design SQUID magnetometer. Crystals of **1**−**3** were extracted from the mother liquor, and then they were immediately introduced at 110 K without vacuum under a continuous He flow to prevent any partial water loss prior to carrying out the magnetic measurements of these "fresh-hydrated" phases. Afterward, the polycrystalline samples of **1**−**3** were kept at 80 °C for 120 min under vacuum to yield the dehydrated phases **1′**−**3′** prior to carrying out the magnetic measurements. The susceptibility data were corrected for the diamagnetism of both the constituent atoms and the sample holder.

■ ASSOCIATED CONTENT

Supporting Information

The Supporting Information is available free of charge on the ACS Publications website at DOI: 10.1021/acs.inorgchem.5b01854.

Preparation and physical characterization data of **2** and **3**, additional structural and magnetic data of **1**−**3** (Figures S1−S14), and crystallographic refinement details for **1**−**3** (Table S1) (PDF)

Crystallographic data for CCDC-1036928 (**2**) (CIF)

Crystallographic data for CCDC-1036929 (**3**) (CIF)

■ AUTHOR INFORMATION

Corresponding Authors

*E-mail: jesus.ferrando@uv.es.

*E-mail: donatella.armentano@unical.it.

*E-mail: emilio.pardo@uv.es.

Notes

The authors declare no competing financial interest.

■ ACKNOWLEDGMENTS

This work was supported by the MINECO (Spain) (Projects CTQ2013-46362-P and CTQ2013-44844-P), the Generalitat Valenciana (Spain) (Project PROMETEOII/2014/070), and the Ministero dell'Istruzione, dell'Università e della Ricerca (Italy). T.G. thanks the Universitat de València for a predoctoral contract. Thanks are also extended to the MICINN Ramón y Cajal Program (E.P.). B.S. and J.G. acknowledge the financial support of the European Research Council under the European Union's Seventh Framework Programme (FP/2007-2013)/ERC Grant Agreement no. 335746, CrystEng-MOF-MMM. We are especially thankful to Dr. Rafael Ruiz-García (Universitat de València) for unselfish help and continuous interest in this work.

■ REFERENCES

(1) Rosi, N. L.; Eddaoudi, M.; Kim, J.; O'Keeffe, M.; Yaghi, O. M. *CrystEngComm* **2002**, *4*, 401−404.

(2) Janiak, C. *Dalton Trans.* **2003**, 2781−2804.

(3) Bradshaw, D.; Claridge, J. B.; Cussen, E. J.; Prior, T. J.; Rosseinsky, M. J. *Acc. Chem. Res.* **2005**, *38*, 273−282.

(4) Kitagawa, S.; Matsuda, R. *Coord. Chem. Rev.* **2007**, *251*, 2490−2509.

DOI: 10.1021/acs.inorgchem.5b01854
Inorg. Chem. XXXX, XXX, XXX−XXX

(5) Férey, G. *Chem. Soc. Rev.* **2008**, *37*, 191−214.
(6) Long, J. R.; Yaghi, O. M. *Chem. Soc. Rev.* **2009**, *38*, 1213−1214.
(7) Coronado, E.; Galán-Mascarós, J. R.; Gómez-García, C. J.; Laukhin, V. *Nature* **2000**, *408*, 447−449.
(8) Train, C.; Gheorghe, R.; Krstic, V.; Chamoreau, L.-M.; Ovanesyan, N. S.; Rikken, G. L. J. A.; Gruselle, M.; Verdaguer, M. *Nat. Mater.* **2008**, *7*, 729−734.
(9) Ohkoshi, S.-I.; Imoto, K.; Tsunobuchi, Y.; Takano, S.; Tokoro, H. *Nat. Chem.* **2011**, *3*, 564−569.
(10) Pardo, E.; Train, C.; Gontard, G.; Boubekeur, K.; Fabelo, O.; Liu, H.; Dkhil, B.; Lloret, F.; Nakagawa, K.; Tokoro, H.; Ohkoshi, S.; Verdaguer, M. *J. Am. Chem. Soc.* **2011**, *133*, 15328−15331.
(11) Kreno, L. E.; Leong, K.; Farha, O. K.; Allendorf, M.; Van Duyne, R. P.; Hupp, J. T. *Chem. Rev.* **2012**, *112*, 1105−1125.
(12) Pardo, E.; Train, C.; Liu, H.; Chamoreau, L.-M.; Dkhil, B.; Boubekeur, K.; Lloret, F.; Nakatani, K.; Tokoro, H.; Ohkoshi, S.; Verdaguer, M. *Angew. Chem., Int. Ed.* **2012**, *51*, 8356−8360.
(13) Maspoch, D.; Ruiz-Molina, D.; Veciana, J. *Chem. Soc. Rev.* **2007**, *36*, 770−818.
(14) Dechambenoit, P.; Long, J. R. *Chem. Soc. Rev.* **2011**, *40*, 3249−3265.
(15) Grancha, T.; Ferrando-Soria, J.; Castellano, M.; Julve, M.; Pasán, J.; Armentano, D.; Pardo, E. *Chem. Commun.* **2014**, *50*, 7569−7585.
(16) *Molecule-Based Magnetic Materials*; Turnbull, M. M., Sugimoto, T., Thompson, L. K., Eds.; ACS Symposium Series; American Chemical Society: Washington, DC, 1996; Vol. *644*.
(17) Yaghi, O. M.; O'Keeffe, M.; Ockwig, N. W.; Chae, H. K.; Eddaoudi, M.; Kim, J. *Nature* **2003**, *423*, 705−714.
(18) Goesten, M. G.; Kapteijn, F.; Gascon, J. *CrystEngComm* **2013**, *15*, 9249−9257.
(19) Brozek, C. K.; Dincă, M. *Chem. Soc. Rev.* **2014**, *43*, 5456−5467.
(20) Cohen, S. M. *Chem. Rev.* **2012**, *112*, 970−1000.
(21) Liu, T.-F.; Zou, L.; Feng, D.; Chen, Y.-P.; Fordham, S.; Wang, X.; Liu, Y.; Zhou, H.-C. *J. Am. Chem. Soc.* **2014**, *136*, 7813−7816.
(22) Grancha, T.; Ferrando-Soria, J.; Zhou, H.-C.; Gascon, J.; Seoane, B.; Pasán, J.; Fabelo, O.; Julve, M.; Pardo, E. *Angew. Chem., Int. Ed.* **2015**, *54*, 6521−6525.
(23) Fei, H.; Cahill, J. F.; Prather, K. a; Cohen, S. M. *Inorg. Chem.* **2013**, *52*, 4011−4016.
(24) Cui, X.; Khlobystov, A. N.; Chen, X.; Marsh, D. H.; Blake, A. J.; Lewis, W.; Champness, N. R.; Roberts, C. J.; Schröder, M. *Chem. - Eur. J.* **2009**, *15*, 8861−8873.
(25) Li, B.; Zhang, Y.; Ma, D.; Ma, T.; Shi, Z.; Ma, S. *J. Am. Chem. Soc.* **2014**, *136*, 1202−1205.
(26) Yao, R.; Xu, X.; Zhang, X. *Chem. Mater.* **2012**, *24*, 303−310.
(27) Zeng, M. H.; Yin, Z.; Tan, Y. X.; Zhang, W. X.; He, Y. P.; Kurmoo, M. *J. Am. Chem. Soc.* **2014**, *136*, 4680−4688.
(28) Dinca, M.; Long, J. R. *J. Am. Chem. Soc.* **2007**, *129*, 11172−11176.
(29) Yang, S.; Lin, X.; Blake, A. J.; Thomas, K. M.; Hubberstey, P.; Champness, N. R.; Schröder, M. *Chem. Commun.* **2008**, *7345*, 6108−6110.
(30) Himsl, D.; Wallacher, D.; Hartmann, M. *Angew. Chem., Int. Ed.* **2009**, *48*, 4639−4642.
(31) Nouar, F.; Eckert, J.; Eubank, J. F.; Forster, P.; Eddaoudi, M. *J. Am. Chem. Soc.* **2009**, *131*, 2864−2870.
(32) Yang, S.; Lin, X.; Blake, A. J.; Walker, G. S.; Hubberstey, P.; Champness, N. R.; Schröder, M. *Nat. Chem.* **2009**, *1*, 487−493.
(33) An, J.; Rosi, N. L. *J. Am. Chem. Soc.* **2010**, *132*, 5578−5579.
(34) Procopio, E. Q.; Linares, F.; Montoro, C.; Colombo, V.; Maspero, A.; Barea, E.; Navarro, J. A. R. *Angew. Chem., Int. Ed.* **2010**, *49*, 7308−7311.
(35) Nohra, B.; El Moll, H.; Rodriguez Albelo, L. M.; Mialane, P.; Marrot, J.; Mellot-Draznieks, C.; O'Keeffe, M.; Ngo Biboum, R.; Lemaire, J.; Keita, B.; Nadjo, L.; Dolbecq, A. *J. Am. Chem. Soc.* **2011**, *133*, 13363−13374.
(36) Yang, S.; Martin, G. S. B.; Titman, J. J.; Blake, A. J.; Allan, D. R.; Champness, N. R.; Schröder, M. *Inorg. Chem.* **2011**, *50*, 9374−9384.
(37) Lin, Z.-J.; Liu, T.-F.; Huang, Y.-B.; Lü, J.; Cao, R. *Chem. - Eur. J.* **2012**, *18*, 7896−7902.
(38) Fei, H.; Rogow, D. L.; Oliver, S. R. J. *J. Am. Chem. Soc.* **2010**, *132*, 7202−7209.
(39) Genna, D. T.; Wong-Foy, A. G.; Matzger, A. J.; Sanford, M. S. *J. Am. Chem. Soc.* **2013**, *135*, 10586−10589.
(40) An, J.; Geib, S. J.; Rosi, N. L. *J. Am. Chem. Soc.* **2009**, *131*, 8376−8377.
(41) An, J.; Shade, C. M.; Chengelis-Czegan, D. a; Petoud, S.; Rosi, N. L. *J. Am. Chem. Soc.* **2011**, *133*, 1220−1223.
(42) Qin, J.-S.; Zhang, S.-R.; Du, D.-Y.; Shen, P.; Bao, S.-J.; Lan, Y.-Q.; Su, Z.-M. *Chem. - Eur. J.* **2014**, *20*, 5625−5630.
(43) Ferrando-Soria, J.; Grancha, T.; Julve, M.; Cano, J.; Lloret, F.; Journaux, Y.; Pasán, J.; Ruiz-Pérez, C.; Pardo, E. *Chem. Commun.* **2012**, *48*, 3539−3541.
(44) Ferrando-Soria, J.; Ruiz-García, R.; Cano, J.; Stiriba, S.-E.; Vallejo, J.; Castro, I.; Julve, M.; Lloret, F.; Amorós, P.; Pasán, J.; Ruiz-Pérez, C.; Journaux, Y.; Pardo, E. *Chem. - Eur. J.* **2012**, *18*, 1608−1617.
(45) Ferrando-Soria, J.; Serra-Crespo, P.; de Lange, M.; Gascon, J.; Kapteijn, F.; Julve, M.; Cano, J.; Lloret, F.; Pasán, J.; Ruiz-Pérez, C.; Journaux, Y.; Pardo, E. *J. Am. Chem. Soc.* **2012**, *134*, 15301−15304.
(46) Ferrando-Soria, J.; Khajavi, H.; Serra-Crespo, P.; Gascon, J.; Kapteijn, F.; Julve, M.; Lloret, F.; Pasán, J.; Ruiz-Pérez, C.; Journaux, Y.; Pardo, E. *Adv. Mater.* **2012**, *24*, 5625−5629.
(47) Grancha, T.; Tourbillon, C.; Ferrando-Soria, J.; Julve, M.; Lloret, F.; Pasán, J.; Ruiz-Pérez, C.; Fabelo, O.; Pardo, E. *CrystEngComm* **2013**, *15*, 9312.
(48) Lozinska, M. M.; Mangano, E.; Mowat, J. P. S.; Shepherd, A. M.; Howe, R. F.; Thompson, S. P.; Parker, J. E.; Brandani, S.; Wright, P. A. *J. Am. Chem. Soc.* **2012**, *134*, 17628−17642.
(49) *SAINT*, version 6.45; Bruker Analytical X-ray Systems, Madison, WI, 2003.
(50) Sheldrick, G. M. *SADABS Program for Absorption Correction*, version 2.10; Analytical X-ray Systems: Madison, WI, 2003.
(51) Li, Q.; Zhang, W.; Miljanić, O. S.; Knobler, C. B.; Stoddart, J. F.; Yaghi, O. M. *Chem. Commun.* **2010**, *46*, 380−382.
(52) Furukawa, H.; Ko, N.; Go, Y. B.; Aratani, N.; Choi, S. B.; Choi, E.; Yazaydin, A. O.; Snurr, R. Q.; O'Keeffe, M.; Kim, J.; Yaghi, O. M. *Science* **2010**, *329*, 424−428.
(53) Smaldone, R. A.; Forgan, R. S.; Furukawa, H.; Gassensmith, J. J.; Slawin, A. M. Z.; Yaghi, O. M.; Stoddart, J. F. *Angew. Chem., Int. Ed.* **2010**, *49*, 8630−8634.
(54) Coskun, A.; Hmadeh, M.; Barin, G.; Gándara, F.; Li, Q.; Choi, E.; Strutt, N. L.; Cordes, D. B.; Slawin, A. M. Z.; Stoddart, J. F.; Sauvage, J. P.; Yaghi, O. M. *Angew. Chem., Int. Ed.* **2012**, *51*, 2160−2163.
(55) Sheldrick, G. M. *Acta Crystallogr., Sect. A: Found. Crystallogr.* **2008**, *64*, 112−122.
(56) *SHELXTL*-2013/4; Bruker Analytical X-ray Instruments: Madison, WI, 2013.
(57) Spek, A. L. *Acta Crystallogr., Sect. D: Biol. Crystallogr.* **2009**, *65*, 148−155.
(58) Palmer, D. *CRYSTAL MAKER*; Cambridge University Technical Services: Cambridge, 1996.
(59) Farrugia, L. J. *J. Appl. Crystallogr.* **1999**, *32*, 837−838.
(60) *POV-Ray*, version 3.6.2; Persistence of Vision Raytracer, Pty. Ltd., 2003.
(61) *X'Pert HighScore Plus*; PANalytical: The Netherlands, 2012.
(62) Brunauer, S.; Emmett, P. H.; Teller, E. *J. Am. Chem. Soc.* **1938**, *60*, 309−319.

DOI: 10.1021/acs.inorgchem.5b01854
Inorg. Chem. XXXX, XXX, XXX−XXX